

Dissipative hydrodynamic equation of a ferromagnetic Bose-Einstein condensate: Analogy to magnetization dynamics in conducting ferromagnets

Kazue Kudo¹ and Yuki Kawaguchi²

¹*Division of Advanced Sciences, Ochanomizu Academic Production,
Ochanomizu University, 2-1-1 Ohtsuka, Bunkyo-ku, Tokyo 112-8610, Japan*

²*Department of Physics, University of Tokyo, 7-3-1 Hongo, Bunkyo-ku, Tokyo 113-0033, Japan*
(Dated: November 9, 2018)

The hydrodynamic equation of a spinor Bose-Einstein condensate (BEC) gives a simple description of spin dynamics in the condensate. We introduce the hydrodynamic equation of a ferromagnetic BEC with dissipation originating from the energy dissipation of the condensate. The dissipative hydrodynamic equation has the same form as an extended Landau-Lifshitz-Gilbert (LLG) equation, which describes the magnetization dynamics of conducting ferromagnets in which localized magnetization interacts with spin-polarized currents. Employing the dissipative hydrodynamic equation, we demonstrate the magnetic domain pattern dynamics of a ferromagnetic BEC in the presence and absence of a current of particles, and discuss the effects of the current on domain pattern formation. We also discuss the characteristic lengths of domain patterns that have domain walls with and without finite magnetization.

PACS numbers: 03.75.Kk, 03.75.Mn 03.75.Lm

I. INTRODUCTION

A particular feature of superfluids and superconductors with spin degrees of freedom, such as superfluid Helium three, p -wave superconductors, and spinor Bose-Einstein condensates (BECs) of ultra-cold atoms, is that they support the non-dissipative flow of spins, or spin supercurrent [1, 2]. In such systems, the condensed state is described with a multi-component order parameter; the supercurrent of the particles in each spin state is proportional to the phase gradient of the corresponding component of the order parameter; hence, the gradient of the relative phase of the order parameters in different spin states yields the supercurrent of spins. In particular, when the system is spontaneously magnetized, the spin supercurrent is expected to give a nontrivial effect on the magnetization dynamics. This is the case for a ferromagnetic BEC. In recent experiments, *in situ* techniques for the imaging of magnetization profiles enables us to investigate the real-time dynamics of magnetizations, such as spin texture formation and the nucleation of spin vortices, in ferromagnetic BECs [3–5].

For the investigation of the magnetization dynamics, a hydrodynamic equation has an advantage. It provides the simple description of magnetization dynamics in a ferromagnetic BEC to investigate instabilities [6, 7] and configurations of skyrmions and spin textures [8, 9]. The hydrodynamic equation, in the absence of energy dissipation, takes the same form as the Landau-Lifshitz-Gilbert (LLG) equation without damping if the partial time derivative is replaced by the material derivative $D_t = \partial_t + \mathbf{v}_{\text{mass}} \cdot \nabla$, or equivalently, if the adiabatic spin-transfer torque is added [10, 11]. Here, \mathbf{v}_{mass} is the superfluid velocity, which is related to the magnetization direction $\hat{\mathbf{f}}$ as

$$\nabla \times \mathbf{v}_{\text{mass}} = \frac{\hbar F}{2M} \hat{\mathbf{f}} \cdot (\nabla \hat{\mathbf{f}} \times \nabla \hat{\mathbf{f}}), \quad (1)$$

where F and M are the spin and mass of an atom, respectively. This identity comes from the continuous spin-gauge symmetry of the ferromagnetic BEC [12, 13], and is known as the Mermin-Ho relation [14]. Since the spin is transferred along the velocity field \mathbf{v}_{mass} [see Eq. (24)], the appearance of \mathbf{v}_{mass} in the hydrodynamic equation is the consequence of the spin supercurrent.

In this paper, we investigate the effect of \mathbf{v}_{mass} on the magnetization dynamics using the hydrodynamic description. We show that in the presence of energy dissipation, the Gross-Pitaevskii (GP) equation for a ferromagnetic BEC is reduced to a dissipative hydrodynamic equation, which is equivalent to the extended LLG equation written as

$$\frac{\partial \hat{\mathbf{f}}}{\partial t} = \frac{1}{\hbar} \hat{\mathbf{f}} \times \mathbf{B}_{\text{eff}} - \Gamma' \hat{\mathbf{f}} \times \frac{\partial \hat{\mathbf{f}}}{\partial t} - (\mathbf{v}_{\text{mass}} \cdot \nabla) \hat{\mathbf{f}}, \quad (2)$$

where \mathbf{B}_{eff} is an effective magnetic field and Γ' is a damping parameter. The standard LLG equation, which is widely used to describe the magnetization dynamics in ferromagnets [15], consists of a spin torque due to the effective magnetic field and a damping term, and it corresponds to Eq. (2) without the third term on the right hand side. The extended LLG equation was introduced to describe the magnetization dynamics affected by spin currents [16],

which includes additional torque terms, the so-called adiabatic [10, 11] and nonadiabatic [17] spin-transfer torques. The third term on the right-hand side of Eq. (2) corresponds to the adiabatic spin torque term. Thus, Eq. (2) is the extended LLG equation without the nonadiabatic spin-transfer torque. In conducting ferromagnets, currents can be controlled by the external field as well as generated by magnetic texture dynamics [18]. In the case of a ferromagnetic BEC, the spin-transfer torques are related to the superfluid velocity \mathbf{v}_{mass} , which is induced by spin textures [see Eq. (1)]. The damping parameter Γ' in Eq. (2) corresponds to the so-called Gilbert damping parameter. The Gilbert damping was introduced originally on a phenomenological basis. However, in a conducting ferromagnet system, the damping parameter can be derived microscopically [19]. In the case of a ferromagnetic BEC, the damping term arises due to collision with non-condensed atoms, which is introduced in a phenomenological manner.

The analogy between the dissipative hydrodynamic equation and the extended LLG equation implies interesting connections between ferromagnetic BECs and conducting ferromagnets. For instance, the current-driven motion of domain walls and spin vortices, which has been investigated in conducting ferromagnets theoretically [17, 20, 21] and experimentally [22, 23], can be investigated also in ferromagnetic BECs by comparison. More interesting phenomena such as the anomalous Hall effect, which is the Hall effect due to the magnetization in a conducting ferromagnet [24–27], may be investigated in a ferromagnetic BEC from the viewpoint of the interaction between current and spin configuration. Since there are no impurities in a ferromagnetic BEC, which is also indicated by the absence of the nonadiabatic term in the hydrodynamic equation, we can expect to investigate pure adiabatic spin-transfer effects in this system. These interesting connections motivated us to investigate the domain wall motion and the effect of the superfluid current in a ferromagnetic BEC. In this paper, we demonstrate the magnetic domain pattern dynamics, which are mainly simulated by the dissipative hydrodynamic equation.

In the study of magnetization dynamics, we take into account the magnetic dipole-dipole interaction (MDDI) and the quadratic Zeeman effect. The MDDI is known to yield the spatial structure of magnetizations [28–31]. On the other hand, the quadratic Zeeman energy determines the easy axis of the magnetization. In this paper, we consider a quasi-two dimensional (2D) system and choose the easy axis normal to the 2D plane. Labyrinthine or striped patterns then appear in the magnetic domains with the magnetization parallel and anti-parallel to the normal direction, similar to the domain patterns in a ferromagnetic thin film [32]. We numerically investigate the domain formation dynamics with and without the superfluid current, and find that the superfluid current helps the spin transport to reach a stationary configuration. We also discuss characteristic lengths of a domain pattern in the stationary state. The analytical estimation of domain size shows good agreement with the averaged domain size of the numerically simulated domain pattern.

The paper is organized as follows. In Sec. II, we derive the dissipative hydrodynamic equation from the GP equation with dissipation. In Sec. III, we explain how the MDDI is implemented in the hydrodynamic equation and which type of magnetic domain pattern is expected to appear depending on the balance between the MDDI energy and the quadratic Zeeman energy. We demonstrate the dynamics of the magnetic domain patterns simulated by the dissipative hydrodynamic equation in Sec. IV. The time evolution of average longitudinal magnetization, kinetic and MDDI energies is also shown for different quadratic Zeeman energies. The domain pattern dynamics are compared between hydrodynamic equation simulations with and without the superfluid current and those of the GP equation. In Sec. V, we theoretically estimate the characteristic lengths of magnetic domain patterns. The characteristic domain size shortly after the emergence of a pattern is estimated from the dynamical instability, and that of the stationary pattern is estimated using an ansatz of a stripe domain configuration. Conclusions and outlook are given in Sec. VI.

II. DISSIPATIVE HYDRODYNAMIC EQUATION

We consider a spin- F BEC of N atoms under a uniform magnetic field applied in the z direction confined in a spin-independent optical trap $U_{\text{trap}}(\mathbf{r})$. The zero-temperature mean-field energy is given by

$$\mathcal{E} = \mathcal{E}_{\text{kin}} + \mathcal{E}_{\text{trap}} + \mathcal{E}_p + \mathcal{E}_q + \mathcal{E}_s + \mathcal{E}_{\text{dd}}, \quad (3)$$

where \mathcal{E}_{kin} , $\mathcal{E}_{\text{trap}}$, \mathcal{E}_p , \mathcal{E}_q , \mathcal{E}_s , and \mathcal{E}_{dd} are the kinetic energy, the trapping potential energy, the linear and quadratic Zeeman energies, the short-range interaction energy, and the MDDI energy, respectively. The kinetic and the trapping potential energies are given by

$$\mathcal{E}_{\text{kin}} = \int d\mathbf{r} \sum_{m=-F}^F \Psi_m^*(\mathbf{r}) \left(-\frac{\hbar^2}{2M} \nabla^2 \right) \Psi_m(\mathbf{r}), \quad (4)$$

$$\mathcal{E}_{\text{trap}} = \int d\mathbf{r} U_{\text{trap}}(\mathbf{r}) \sum_{m=-F}^F |\Psi_m(\mathbf{r})|^2, \quad (5)$$

respectively, where $\Psi_m(\mathbf{r})$ is the condensate wave function for the atoms in the magnetic sublevel m . The wave function is normalized to satisfy

$$N = \int d\mathbf{r} \sum_{m=-F}^F |\Psi_m(\mathbf{r})|^2. \quad (6)$$

The linear and quadratic Zeeman energies under the external magnetic field $\mathbf{B} = B\hat{z}$ are given by

$$\mathcal{E}_p = p \int d\mathbf{r} \sum_{m,n=-F}^F \Psi_m^*(\mathbf{r})(F_z)_{mn}\Psi_n(\mathbf{r}), \quad (7)$$

$$\mathcal{E}_q = q \int d\mathbf{r} \sum_{m,n=-F}^F \Psi_m^*(\mathbf{r})(F_z^2)_{mn}\Psi_n(\mathbf{r}), \quad (8)$$

respectively. Here, $F_{x,y,z}$ are the spin- F matrices. The linear Zeeman energy per atom is given by $p = g_F\mu_B B$, where g_F is the hyperfine g -factor, and μ_B is the Bohr magneton. The quadratic Zeeman energy is induced by a linearly polarized microwave field as well as by an external magnetic field: $q = q_B + q_{EM}$, where $q_B = (g_F\mu_B B)^2/E_{hf}$, with E_{hf} being the hyperfine splitting energy, and $q_{EM} = -\hbar^2\Omega^2/(4\delta)$, with Ω being the Rabi frequency and δ the detuning [33].

The short-range interaction energy is

$$\mathcal{E}_s = \frac{1}{2} \int d\mathbf{r} \sum_{m,n} \sum_{m',n'} \Psi_m^*(\mathbf{r})\Psi_{m'}^*(\mathbf{r}) \sum_{S=0,\text{even}}^{2F} \sum_{M_S=-S}^S \frac{4\pi\hbar^2}{M} a_S \langle Fm, Fm' | SM_S \rangle \langle SM_S | Fn', Fn \rangle \Psi_{n'}(\mathbf{r})\Psi_n(\mathbf{r}), \quad (9)$$

which comes from the short-range part of the two-body interaction given by

$$V_s(\mathbf{r}, \mathbf{r}') = \delta(\mathbf{r} - \mathbf{r}') \sum_{S=0,\text{even}}^{2F} \frac{4\pi\hbar^2}{M} a_S \mathcal{P}_S, \quad (10)$$

where $\mathcal{P}_S = \sum_{M_S=-S}^S |SM_S\rangle\langle SM_S|$ projects a pair of spin- F atoms onto the state with total spin S , a_S is the s -wave scattering length for the corresponding spin channel S , and $\langle Fm, Fn | SM_S \rangle$ in Eq. (10) is the Clebsch-Gordan coefficient.

The MDDI energy is given by

$$\mathcal{E}_{dd} = \frac{c_{dd}}{2} \int d\mathbf{r} d\mathbf{r}' \sum_{\mu,\nu=x,y,z} f_\mu(\mathbf{r}) Q_{\mu\nu}(\mathbf{r} - \mathbf{r}') f_\nu(\mathbf{r}'), \quad (11)$$

where $c_{dd} = \mu_0(g_F\mu_B)^2/(4\pi)$, with μ_0 being the magnetic permeability of the vacuum, $Q_{\mu\nu}(\mathbf{r})$ is the dipole kernel, whose detailed form is given in the next section, and

$$f_\mu(\mathbf{r}) = \sum_{m,n=-F}^F \Psi_m^*(\mathbf{r})(F_\mu)_{mn}\Psi_n(\mathbf{r}) \quad (12)$$

is the spin density. The number density is defined by

$$n_{\text{tot}}(\mathbf{r}) = \sum_{m=-F}^F |\Psi_m(\mathbf{r})|^2. \quad (13)$$

The hydrodynamic equation without dissipation has been derived from the GP equation [6–8]. Here, we consider dissipation, which can be phenomenologically introduced to the GP equation by replacing $i\partial/\partial t$ with $(i - \Gamma)\partial/\partial t$ [34]. The origin of the dissipation can be interpreted as the relaxation process of the thermal particles into the condensate [34, 35]. The value of Γ is often taken to be 0.03, and, in fact, experimental results have been well explained by the dissipative equation with $\Gamma = 0.03$ [34, 35]. The dissipative GP equation is given by

$$\begin{aligned} (i - \Gamma)\hbar \frac{\partial}{\partial t} \Psi_m(\mathbf{r}, t) &= \frac{\delta(\mathcal{E} - N\mu(t))}{\delta\Psi_m^*(\mathbf{r}, t)} \\ &= \sum_{n=-F}^F \left[-\frac{\hbar^2}{2M} \nabla^2 \delta_{mn} + H_{mn}(\mathbf{r}, t) - \mu(t)\delta_{mn} \right] \Psi_n(\mathbf{r}, t), \end{aligned} \quad (14)$$

where we use the time-dependent chemical potential $\mu(t)$ so that the total number of atoms is conserved. The spin-dependent part H_{mn} is given by

$$\begin{aligned} H_{mn}(\mathbf{r}, t) &= U_{\text{trap}}(\mathbf{r})\delta_{mn} + p(F_z)_{mn} + q(F_z^2)_{mn} \\ &+ \sum_{m', n'=-F}^F \sum_{S=0, \text{even}}^{2F} \sum_{M_S=-S}^S \frac{4\pi\hbar^2}{M} a_S \langle Fm, Fm' | SM_S \rangle \langle SM_S | Fn', Fn \rangle \Psi_{m'}^*(\mathbf{r}, t) \Psi_{n'}(\mathbf{r}, t) \\ &+ c_{\text{dd}} \sum_{\mu=x, y, z} b_\mu(\mathbf{r}, t) (F_\mu)_{mn}, \end{aligned} \quad (15)$$

where the non-local dipole field $\mathbf{b}(\mathbf{r}, t)$ is defined by

$$b_\mu(\mathbf{r}, t) = \int d\mathbf{r}' \sum_{\nu=x, y, z} Q_{\mu\nu}(\mathbf{r} - \mathbf{r}') f_\nu(\mathbf{r}', t). \quad (16)$$

Below we omit the summation symbol: Greek indices that appear twice are to be summed over $x, y,$ and $z,$ and Roman indices are to be summed over $-F, \dots, F.$

In the following, we consider a ferromagnetic BEC. We assume that the BEC is fully magnetized, $|\mathbf{f}| = Fn_{\text{tot}},$ and only the direction of the spin density can vary in space. This assumption is valid when the ferromagnetic interaction energy is sufficiently large in comparison with the other spinor interaction energies, MDDI energy, quadratic Zeeman energy, and the kinetic energy arising from the spacial variation of the direction of $\mathbf{f}.$ The linear Zeeman effect is not necessarily weaker than the ferromagnetic interaction, since it merely induces the Larmor precession. For example, the short-range interaction (10) for a spin-1 BEC can be written as (see Appendix B 2)

$$\langle mn | V_s(\mathbf{r}, \mathbf{r}') | m' n' \rangle = \delta(\mathbf{r} - \mathbf{r}') [c_0 \delta_{mn} \delta_{m' n'} + c_1 (F_\mu)_{mn} (F_\mu)_{m' n'}], \quad (17)$$

where $c_0 = 4\pi\hbar^2(2a_2 + a_0)/(3M)$ and $c_1 = 4\pi\hbar^2(a_2 - a_0)/(3M).$ The ground state is ferromagnetic for $c_1 < 0.$ The above assumption is valid when $|q| \ll |c_1| n_{\text{tot}}, c_{\text{dd}} \ll |c_1|,$ and the length scale of the spatial spin structure is larger than the spin healing length $\xi_{\text{sp}} = \hbar/\sqrt{2M|c_1|n_{\text{tot}}}.$ Moreover, in the incompressible limit, namely when the spin-independent interaction ($c_0 n_{\text{tot}}$ for the case of a spin-1 BEC) is much stronger than the ferromagnetic interaction and MDDI, the number density n_{tot} is determined, regardless of the spin structure, and assumed to be stationary. This is the case for the spin-1 ^{87}Rb BEC.

We introduce a normalized spinor ζ_m with $\Psi_m(\mathbf{r}, t) = \sqrt{n_{\text{tot}}(\mathbf{r}, t)} \zeta_m(\mathbf{r}, t).$ When the atomic spin is polarized in the z direction, the order parameter is given by $\zeta_m^{(0)} = \delta_{mF}.$ The general order parameter is obtained by performing the gauge transformation and Euler rotation as

$$\begin{aligned} \zeta_m &= e^{i\phi} e^{-iF_z\alpha} e^{-iF_y\beta} e^{-iF_z\gamma} \zeta_m^{(0)} \\ &= e^{i(\phi-F\gamma)} e^{-iF_z\alpha} e^{-iF_y\beta} \zeta_m^{(0)} \\ &\equiv e^{i(\phi-F\gamma)} U \zeta_m^{(0)}, \end{aligned} \quad (18)$$

where $\alpha, \beta,$ and γ are Euler angles and ϕ is the overall phase. Due to the spin-gauge symmetry of the ferromagnetic BEC (i.e., the equivalence between the phase change ϕ and spin rotation γ), distinct configurations of ζ_m are characterized with a set of parameters $\alpha, \beta,$ and $\phi' \equiv \phi - F\gamma.$ The unit vector of the spin density, $\hat{\mathbf{f}} \equiv \mathbf{f}/(Fn_{\text{tot}}),$ for the order parameter (18) is denoted by α and $\beta:$

$$\begin{aligned} \hat{\mathbf{f}} &= \frac{1}{F} \zeta_m^* \mathbf{F}_{mn} \zeta_n \\ &= \frac{1}{F} \zeta_m^{(0)*} (U^\dagger \mathbf{F} U)_{mn} \zeta_n^{(0)} \\ &= \frac{1}{F} \mathcal{R} [\zeta_m^{(0)*} \mathbf{F}_{mn} \zeta_n^{(0)}] \\ &= \begin{pmatrix} \sin \beta \cos \alpha \\ \sin \beta \sin \alpha \\ \cos \beta \end{pmatrix}, \end{aligned} \quad (19)$$

where \mathcal{R} is an SO(3) rotation matrix given by

$$\mathcal{R} = \begin{pmatrix} \cos \alpha & -\sin \alpha & 0 \\ \sin \alpha & \cos \alpha & 0 \\ 0 & 0 & 1 \end{pmatrix} \begin{pmatrix} \cos \beta & 0 & \sin \beta \\ 0 & 1 & 0 \\ -\sin \beta & 0 & \cos \beta \end{pmatrix}. \quad (20)$$

The time evolutions of the total number density and the normalized spin density are given by

$$\frac{\partial n_{\text{tot}}}{\partial t} = \Psi_m^* \left(\frac{\partial}{\partial t} \Psi_m \right) + \left(\frac{\partial}{\partial t} \Psi_m^* \right) \Psi_m, \quad (21)$$

$$\frac{\partial \hat{\mathbf{f}}}{\partial t} = \frac{1}{Fn_{\text{tot}}} \left[\Psi_m^* \mathbf{F}_{mn} \left(\frac{\partial}{\partial t} \Psi_n \right) + \left(\frac{\partial}{\partial t} \Psi_m^* \right) \mathbf{F}_{mn} \Psi_n \right] - \frac{\partial n_{\text{tot}}}{\partial t} \frac{\hat{\mathbf{f}}}{n_{\text{tot}}}, \quad (22)$$

respectively. The velocities of the superfluid current and spin superfluid current are defined by

$$\begin{aligned} \mathbf{v}_{\text{mass}} &= \frac{\hbar}{2Mi} [\zeta_m^* (\nabla \zeta_m) - (\nabla \zeta_m^*) \zeta_m] \\ &= \frac{\hbar}{M} [\nabla \phi' - F(\nabla \alpha) \cos \beta], \end{aligned} \quad (23)$$

$$\begin{aligned} \mathbf{v}_{\text{spin}}^\mu &= \frac{\hbar}{2Mi} (F_\mu)_{mn} [\zeta_m^* (\nabla \zeta_n) - (\nabla \zeta_m^*) \zeta_n] \\ &= F \mathbf{v}_{\text{mass}} \hat{f}_\mu - \frac{\hbar F}{2M} (\hat{\mathbf{f}} \times \nabla \hat{\mathbf{f}})_\mu, \end{aligned} \quad (24)$$

respectively. Substituting Eq.(14) into Eq. (21), we obtain

$$\frac{\partial n_{\text{tot}}}{\partial t} = -\frac{1}{1+\Gamma^2} \nabla \cdot (n_{\text{tot}} \mathbf{v}_{\text{mass}}) - \frac{\Gamma}{1+\Gamma^2} \frac{2}{\hbar} n_{\text{tot}} [\mu_{\text{local}} - \mu(t)], \quad (25)$$

where

$$\mu_{\text{local}} = \frac{\Psi_m^* H_{mn} \Psi_n}{n_{\text{tot}}} - \frac{\hbar^2}{2M} \frac{\nabla^2 \sqrt{n_{\text{tot}}}}{\sqrt{n_{\text{tot}}}} + \frac{M}{2} \mathbf{v}_{\text{mass}}^2 + \frac{\hbar^2 F}{4M} (\nabla \hat{\mathbf{f}})^2. \quad (26)$$

From the above equations, we can also derive the time derivative of \mathbf{v}_{mass} :

$$M \frac{\partial}{\partial t} \mathbf{v}_{\text{mass}} = -\nabla \left[\frac{\mu_{\text{local}} - \mu(t)}{1+\Gamma^2} - \frac{\Gamma}{1+\Gamma^2} \frac{\hbar}{2n_{\text{tot}}} \nabla \cdot (n_{\text{tot}} \mathbf{v}_{\text{mass}}) \right] + \hbar F (\nabla \hat{\mathbf{f}}) \cdot \left(\hat{\mathbf{f}} \times \frac{\partial \hat{\mathbf{f}}}{\partial t} \right). \quad (27)$$

The detailed derivation is given in Appendix A.

Next, we consider the incompressible limit and assume $\partial n_{\text{tot}}/\partial t = 0$. Then, Eq. (25) leads to

$$\nabla \cdot (n_{\text{tot}} \mathbf{v}_{\text{mass}}) = -\frac{2}{\hbar} \Gamma n_{\text{tot}} [\mu_{\text{local}} - \mu(t)]. \quad (28)$$

This equation simplifies Eq. (27):

$$M \frac{\partial}{\partial t} \mathbf{v}_{\text{mass}} = \frac{\hbar}{2n_{\text{tot}} \Gamma} \nabla [\nabla \cdot (n_{\text{tot}} \mathbf{v}_{\text{mass}})] + \hbar F (\nabla \hat{\mathbf{f}}) \cdot \left(\hat{\mathbf{f}} \times \frac{\partial \hat{\mathbf{f}}}{\partial t} \right). \quad (29)$$

Substituting Eq.(14) into Eq. (22) and using Eq. (28), we obtain the equation of motion for spin as follows:

$$\frac{\partial \hat{\mathbf{f}}}{\partial t} = \frac{1}{1+\Gamma^2} \left[\frac{1}{\hbar} \hat{\mathbf{f}} \times \mathbf{B}_{\text{eff}} - (\mathbf{v}_{\text{mass}} \cdot \nabla) \hat{\mathbf{f}} \right] - \frac{\Gamma}{1+\Gamma^2} \hat{\mathbf{f}} \times \left[\frac{1}{\hbar} \hat{\mathbf{f}} \times \mathbf{B}_{\text{eff}} - (\mathbf{v}_{\text{mass}} \cdot \nabla) \hat{\mathbf{f}} \right], \quad (30)$$

$$\mathbf{B}_{\text{eff}} = \frac{\hbar^2}{2M} \nabla^2 \hat{\mathbf{f}} + \frac{\hbar^2}{2M} (\mathbf{a} \cdot \nabla) \hat{\mathbf{f}} - c_{\text{dd}} \mathbf{b} - p \hat{z} - q(2F-1) \hat{f}_z \hat{z}, \quad (31)$$

where $\mathbf{a} = (\nabla n_{\text{tot}})/n_{\text{tot}}$. The detailed derivation is given in Appendix B. The effective field \mathbf{B}_{eff} is also derived from the reduced Hamiltonian \mathcal{H}_{mag} that contains only spin-dependent terms: $F \mathbf{B}_{\text{eff}} = -\delta \mathcal{H}_{\text{mag}}/\delta \hat{\mathbf{f}}$, where

$$\mathcal{H}_{\text{mag}} = \frac{1}{n_{\text{tot}}} \int dr \left\{ \frac{\hbar^2}{4M} \frac{(\nabla \mathbf{f})^2}{Fn_{\text{tot}}} + \frac{c_{\text{dd}}}{2} \mathbf{b} \cdot \mathbf{f} + p \hat{z} \cdot \mathbf{f} + \frac{q}{2} \frac{(2F-1)}{Fn_{\text{tot}}} (\hat{z} \cdot \mathbf{f})^2 \right\}, \quad (32)$$

and \mathbf{b} includes \mathbf{f} .

Here we note that Eq. (30) is equivalent to Eq. (2) and corresponds to the extended LLG equation, which describes the magnetization dynamics in a conducting ferromagnet in the presence of spin currents interacting with magnetization, with the adiabatic spin-transfer torque. The superfluid velocity \mathbf{v}_{mass} in Eq. (30) corresponds to the spin current, which is associated with the electric current density in the extended LLG equation of a conducting ferromagnet.

III. MAGNETIC DIPOLE-DIPOLE INTERACTION

Below, we consider a BEC confined in a quasi-2D trap whose Thomas-Fermi radius in the z direction is smaller than the spin healing length. We approximate the wave function in the z direction by a Gaussian with width d : $\Psi_m(\mathbf{r}_\perp, z) = \psi_m(\mathbf{r}_\perp)h(z)$, where $\mathbf{r}_\perp \equiv (x, y)$, and $h(z) = \exp[-z^2/(4d^2)]/(2\pi d^2)^{1/4}$. When we consider a quasi-2D BEC, n_{tot} , $\hat{\mathbf{f}}$, and \mathbf{v}_{mass} are defined by means of ψ_m instead of Ψ_m [36]. If one replaces Ψ_m with ψ_m , a_S with ηa_S , c_{dd} with ηc_{dd} , and \mathbf{b} with $\bar{\mathbf{b}}$, the equation is the same as Eq. (14), where $\eta = \int dz h^4(z) / \int dz h^2(z) = 1/\sqrt{4\pi d^2}$ and

$$\bar{b}_\mu(\mathbf{r}_\perp) = \int d^2 r'_\perp Q_{\mu\nu}^{(2D)}(\mathbf{r}_\perp - \mathbf{r}'_\perp) [\psi_m^*(\mathbf{r}'_\perp)(F_\nu)_{mn}\psi_n(\mathbf{r}'_\perp)], \quad (33)$$

with

$$Q_{\mu\nu}^{(2D)}(\mathbf{r}_\perp - \mathbf{r}'_\perp) = \frac{1}{\eta} \iint dz dz' h^2(z) h^2(z') Q_{\mu\nu}(\mathbf{r} - \mathbf{r}'). \quad (34)$$

The 2D dipole kernel in the laboratory frame of reference is given by

$$Q_{\mu\nu}^{(2D, \text{lab})}(\mathbf{r}) = \sum_{\mathbf{k}} e^{i\mathbf{k}\cdot\mathbf{r}} \tilde{Q}_{\mathbf{k}\mu\nu}^{(2D, \text{lab})}, \quad (35)$$

where the subscript \perp is omitted for simplicity and

$$\tilde{Q}_{\mathbf{k}}^{(2D, \text{lab})} = -\frac{4\pi}{3} \begin{pmatrix} 1 & 0 & 0 \\ 0 & 1 & 0 \\ 0 & 0 & -2 \end{pmatrix} + 4\pi G(kd) \begin{pmatrix} \hat{k}_x^2 & \hat{k}_x \hat{k}_y & 0 \\ \hat{k}_x \hat{k}_y & \hat{k}_y^2 & 0 \\ 0 & 0 & -1 \end{pmatrix}, \quad (36)$$

with $\mathbf{k} = (k_x, k_y)$, $k = |\mathbf{k}|$, $\hat{k}_{x,y} = k_{x,y}/k$, and $G(k) \equiv 2ke^{k^2} \int_k^\infty e^{-t^2} dt = \sqrt{\pi} k e^{k^2} \text{erfc}(k)$. It can be shown that $G(k)$ is a monotonically increasing function that satisfies $G(0) = 0$ and $G(\infty) = 1$.

When the linear Zeeman energy is much larger than the MDDI energy, we choose the rotating frame of reference in spin space by replacing Ψ_m with $e^{-ipmt/\hbar}\Psi_m$, and eliminate the linear Zeeman term from the GP equation. In this case, the contribution of the MDDI is time averaged due to the Larmor precession. The 2D dipole kernel, which is averaged over the Larmor precession period, under an external magnetic field in the z direction, is given by [36]

$$Q_{\mu\nu}^{(2D, \text{rot})}(\mathbf{r}) = (\delta_{\mu\nu} - 3\delta_{z\mu}\delta_{z\nu}) \sum_{\mathbf{k}} e^{i\mathbf{k}\cdot\mathbf{r}} \tilde{Q}_{\mathbf{k}}, \quad (37)$$

where

$$\tilde{Q}_{\mathbf{k}} = \frac{2\pi}{3} [-2 + 3G(kd)]. \quad (38)$$

The formation of a stable magnetic domain pattern depends on the quadratic energy as well as the MDDI. Since the quadratic Zeeman energy is the monotonic function of $q(\hat{z} \cdot \hat{\mathbf{f}})^2$, transverse ($\hat{f}_z = 0$) and longitudinal ($\hat{f}_z = \pm 1$) magnetization is preferable for $q > 0$ and $q < 0$, respectively. For $q > 0$, the uniform pattern of transverse magnetization is stable because of the MDDI. When a strong magnetic field is applied, the dipole kernel is given by Eq. (37), which is low for small- k modes of a transverse magnetization pattern and for large- k modes of a longitudinal one. Thus, a uniform transverse magnetization pattern (i.e., $k = 0$) is stable for $q > 0$. The situation is the same for a magnetic pattern under zero field, in which the dipole kernel is given by Eq. (35). For $q < 0$, the uniform transverse magnetization pattern is still stable if the quadratic Zeeman energy is smaller than the MDDI energy. When $q < 0$ and $|q|$ is large enough to balance with the MDDI, the uniform transverse magnetization becomes unstable and a longitudinal magnetization pattern appears. In other words, there is a threshold of q where a non-uniform longitudinal magnetization pattern appears. The threshold can be calculated from the linear stability analysis, as will be discussed in Sec. V.

Here, we focus on the negative- q regime, which can be achieved by means of a linearly polarized microwave field even in the absence of an external magnetic field [see, below Eq. (8)]. When $q < 0$ and $|q|$ is sufficiently large, longitudinal magnetization is dominant and magnetic domains with $\hat{f}_z \simeq \pm 1$ form patterns because of the MDDI. This situation is consistent with that of a uni-axial ferromagnet [32].

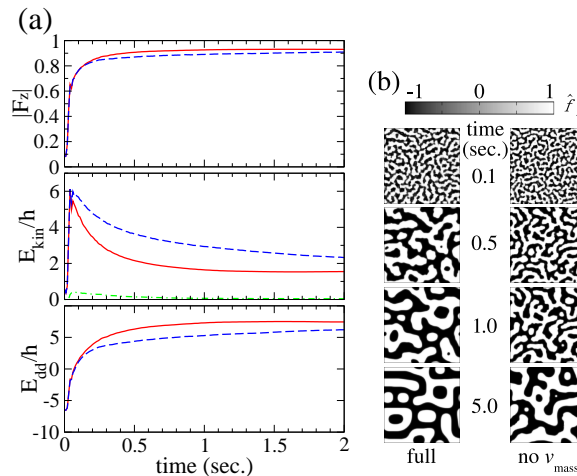


FIG. 1: (Color online) (a) Time dependence of the averaged longitudinal magnetization, kinetic and MDDI energies in the presence (solid curves) and absence (dashed curves) of \mathbf{v}_{mass} . The dot-dashed curve in the graph of E_{kin}/h (middle panel) corresponds to the contribution from \mathbf{v}_{mass} . (b) Snapshots of longitudinal magnetization in which white and black correspond to positive and negative values of \hat{f}_z , respectively. The size of each snapshot is $256 \times 256 \mu\text{m}$. Here, we take $q/h = -50 \text{ Hz}$, and $n_{\text{tot}} = 6n_{\text{tot}}^{(0)}$, where $n_{\text{tot}}^{(0)} = \sqrt{2\pi d^2 n_{3\text{D}}^{(0)}}$ with $n_{3\text{D}}^{(0)} = 2.3 \times 10^{14} \text{ cm}^{-3}$ and $d = 1.0 \mu\text{m}$. The damping rate is given by a typical value $\Gamma = 0.03$. The other parameters are given by the typical values for a spin-1 ^{87}Rb atom: $M = 1.44 \times 10^{-25} \text{ Kg}$, $F = 1$, and $g_F = -1/2$.

IV. DOMAIN FORMATION DYNAMICS

In this section, we focus on the domain formation dynamics with and without \mathbf{v}_{mass} under a strong magnetic field to illustrate how \mathbf{v}_{mass} affects domain pattern formation. Later, the domain patterns under zero magnetic field are also shown as complementary results. The validity of the dissipative hydrodynamic equation is also examined by comparing hydrodynamic and GP equation simulations.

For the magnetic domain pattern simulations, we solve the coupled equations (29) and (30), where \mathbf{v}_{mass} and \mathbf{B}_{eff} are defined by Eqs. (23), and (31), respectively. For simplicity, we take $\mathbf{a} = 0$ and use periodic boundary conditions. In the case of a strong magnetic field, we employ Eq. (37) as a dipole kernel. To see the role of \mathbf{v}_{mass} , we demonstrate the calculation without \mathbf{v}_{mass} , in which \mathbf{v}_{mass} is always taken to be zero, as well as the full calculation using all those equations in the presence of \mathbf{v}_{mass} . The initial condition is $\hat{f}_x \simeq 1$, $\hat{f}_y \simeq 0$, and $\hat{f}_z \simeq 0$ with small noises, and $\mathbf{v}_{\text{mass}} = 0$.

Figure 1(a) shows that the longitudinal magnetization grows rapidly to form magnetic domains. The kinetic and MDDI energies also grow rapidly at first. After the rapid increase, the kinetic energy decays as magnetic domains grow and the domain wall density decreases. The averaged longitudinal magnetization, kinetic energy and its contribution from \mathbf{v}_{mass} , and MDDI energy (per unit area per atom) are defined by

$$\overline{|\hat{f}_z|} = \frac{1}{L^2} \int d^2r |\hat{f}_z(\mathbf{r})|, \quad (39)$$

$$E_{\text{kin}} = E_{\text{flow}} + \frac{1}{L^2} \int d^2r \frac{\hbar^2}{4M} \left[(\nabla \hat{f}_x(\mathbf{r}))^2 + (\nabla \hat{f}_y(\mathbf{r}))^2 + (\nabla \hat{f}_z(\mathbf{r}))^2 \right], \quad (40)$$

$$E_{\text{flow}} = \frac{1}{L^2} \int d^2r \frac{M}{2} \mathbf{v}_{\text{mass}}(\mathbf{r})^2, \quad (41)$$

$$E_{\text{dd}} = \frac{1}{L^2} \int d^2r \frac{c_{\text{dd}}}{2} \eta \bar{\mathbf{b}}(\mathbf{r}) \cdot \hat{\mathbf{f}}(\mathbf{r}), \quad (42)$$

respectively. Here, L is the system size.

The longitudinal magnetization grows rapidly for a short time, and then the averaged longitudinal magnetization saturates at around $|\overline{\hat{f}_z}| \simeq 1$ [see the top panel of Fig. 1(a)]. Figure 1(b) shows that magnetic domains emerge in a short time and, after that, spread slowly to reach a stationary configuration. After the rapid growth of \hat{f}_z , magnetic domain patterns grow faster in the presence than in the absence of \mathbf{v}_{mass} . The difference is apparent in the series of snapshots and E_{kin} and E_{dd} , although the contribution of \mathbf{v}_{mass} to E_{kin} is small compared with the total kinetic energy [see the middle panel of Fig. 1(a)]. In the presence of \mathbf{v}_{mass} , magnetic domains grow efficiently because of spin

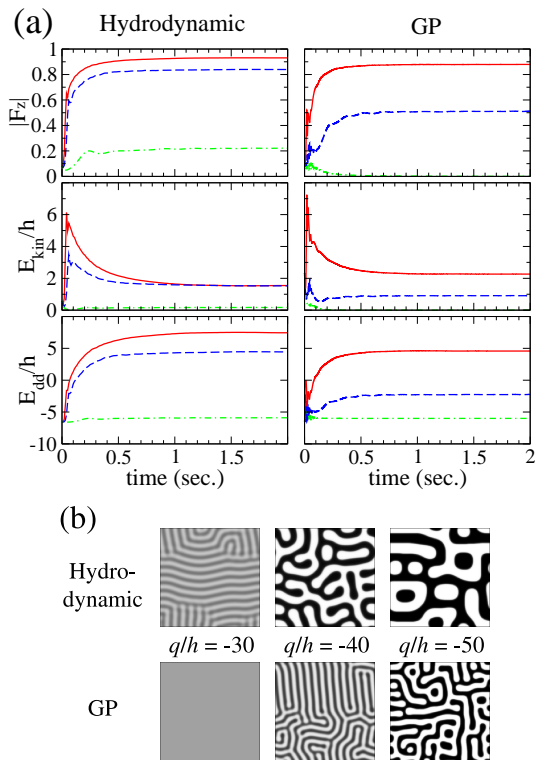


FIG. 2: (Color online) Comparison of domain formation dynamics between the hydrodynamic description and GP numerics. (a) Time dependence of the averaged longitudinal magnetization, kinetic and MDDI energies simulated by the hydrodynamic equation (left column) and the GP equation (right column). (b) Snapshots at $t = 5$ s simulated by the hydrodynamic and GP equations. Solid, dashed, and dot-dashed curves in (a) are for $q/h = -50$, -40 , and -30 , respectively.

transfer accompanied by the transfer of atoms by means of \mathbf{v}_{mass} .

To examine the validity of the hydrodynamic description, we compare the simulations of the dissipative hydrodynamic and the GP equations. In both cases, the averaged $|\hat{f}_z|$, E_{kin} , E_{dd} , and snapshots for several values of q are shown in Fig. 2. For the GP equation, the averaged longitudinal magnetization, kinetic and MDDI energies (per unit area per atom) are defined by

$$\overline{|\hat{f}_z|} = \frac{1}{L^2} \int d^2r \frac{|f_z(\mathbf{r})|}{n_{\text{tot}}(\mathbf{r})}, \quad (43)$$

$$E_{\text{kin}} = \frac{1}{L^2} \frac{1}{N} \left(-\frac{\hbar^2}{2M} \right) \int d^2r \sum_m \psi_m^*(\mathbf{r}) \nabla^2 \psi_m(\mathbf{r}), \quad (44)$$

$$E_{\text{dd}} = \frac{1}{L^2} \frac{1}{N} \int d^2r \frac{c_{\text{dd}}}{2} \eta \bar{\mathbf{b}}(\mathbf{r}) \cdot \mathbf{f}(\mathbf{r}), \quad (45)$$

respectively. Here \mathbf{f} and n_{tot} are defined in Eqs. (12) and (13), respectively. These values are equal to Eqs. (39), (40), and (42) if n_{tot} is uniform and $|\mathbf{f}(\mathbf{r})| = n_{\text{tot}}$. Below the threshold where a non-uniform pattern begins to appear, the most stable pattern is a uniform pattern. The threshold is $q/h \simeq -30$ for the hydrodynamic description and $q/h \simeq -40$ for the GP equation. Near the threshold, the averaged longitudinal magnetization is small compared to those in other cases. Except for in the vicinity of the threshold, the time dependence of domain pattern formation looks similar for the two simulations. However, the domain size differs significantly due to differences in the domain wall structure. In the GP simulation, the amplitude of magnetization is suppressed in domain walls, while the suppression of magnetization does not occur in the hydrodynamic description. An analysis of domain sizes for both cases will be given in the next section.

The magnetic domain patterns under zero field are simulated by the dissipative hydrodynamic equations with Eq. (36). In Fig. 3, domain pattern formation from the initial condition of $\hat{f}_x \simeq 1$ is shown in the presence and in the absence of \mathbf{v}_{mass} . The magnetic domain patterns under zero field look similar to those under a strong magnetic field. The effect of \mathbf{v}_{mass} is also similar: \mathbf{v}_{mass} moves the domain walls faster. However, they are strongly affected by

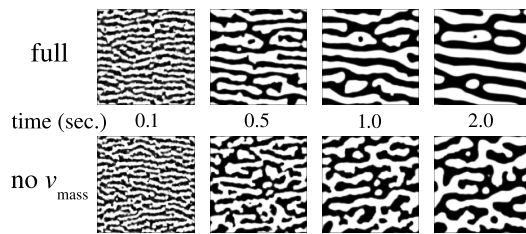


FIG. 3: Domain pattern formation in the absence of a magnetic field. The direction of the stripes depends on the initial configuration of spins. The parameters are the same as those given in Fig. 1

the initial condition. This is because the spin and orbit degrees of freedom couple in the MDDI under zero field [see Eq. (36)]. If the initial condition is given by $\hat{f}_y \simeq 1$, one can see remarkably similar domain patterns as shown in the snapshots in Fig. 3, which are rotated by 90° .

V. CHARACTERISTIC LENGTHS OF DOMAIN PATTERNS

We have seen in the previous section that the magnetic domain pattern has an initially short characteristic length that later increases in size. At the beginning of domain pattern formation, domain size is estimated from the linear instability analysis. The domain size of the stationary pattern can be estimated as that of a stripe domain pattern. For the parameters given in our numerical simulations, the domain size of the stable stripe pattern is longer than the domain size estimated from the linear instability.

A. Dynamical instability

The dynamical instability (linear instability) under a strong magnetic field has been discussed previously, both for the hydrodynamic equation [7] and for the GP equation [36]. For the hydrodynamic equation, the growth rate of the unstable mode is calculated from the eigenvalues of the linearized equation of small deviations from the uniform initial condition. For the GP equation, a similar equation is derived by means of Bogoliubov analysis. When the initial magnetic pattern is uniform and $\hat{f}_x = 1$, the respective growth rates of the unstable mode for the hydrodynamic and GP equations are given by

$$\lambda^H(k) = \sqrt{\left[-\frac{\hbar^2 k^2}{2M} - q - 4\pi c_{\text{dd}} \tilde{n}_{\text{tot}} [1 - G(kd)] \right] \left[\frac{\hbar^2 k^2}{2M} + 2\pi c_{\text{dd}} \tilde{n}_{\text{tot}} G(kd) \right]}, \quad (46)$$

$$\lambda^G(k) = \sqrt{\left[-\frac{\hbar^2 k^2}{2M} - q - 4\pi c_{\text{dd}} \tilde{n}_{\text{tot}} (1 - \tilde{q}) [1 - G(kd)] \right] \left[\frac{\hbar^2 k^2}{2M} + 2\pi c_{\text{dd}} \tilde{n}_{\text{tot}} (1 + \tilde{q}) G(kd) \right]}, \quad (47)$$

where $\tilde{n}_{\text{tot}} = n_{\text{tot}} \eta$ and

$$\tilde{q} = \frac{q}{2\tilde{n}_{\text{tot}}(|c_1| + 4\pi c_{\text{dd}}/3)}. \quad (48)$$

Here, we have considered $\mathbf{v}_{\text{mass}} = 0$ and neglected the dissipation, which is very small (i.e., $\Gamma \ll 1$).

The domain size at the emergence of a non-uniform pattern is estimated as

$$\ell_i = \pi/k_0, \quad (49)$$

where k_0 is given by the momentum at which $\lambda^H(\mathbf{k}_0)$ or $\lambda^G(\mathbf{k}_0)$ has its maximum value.

B. Domain size estimated from the hydrodynamic equation

Here, we estimate characteristic lengths of the domain pattern in the stationary state. For $q < 0$ with large $|q|$, the ideal stable pattern is the stripe pattern of longitudinal magnetization. We assume that the stable pattern is

described by

$$\hat{f}_x = \text{cn}(x/\kappa\xi, \kappa^2), \quad \hat{f}_y = 0, \quad \hat{f}_z = \text{sn}(x/\kappa\xi, \kappa^2), \quad (50)$$

where $\text{sn}(x/\kappa\xi, \kappa^2)$ and $\text{cn}(x/\kappa\xi, \kappa^2)$ are the Jacobi elliptic functions with $0 < \kappa^2 \leq 1$. These functions contain the characteristic lengths of the stripe domain pattern [37]: the domain wall width ξ and the periodicity of the pattern $2\ell_s$ with

$$\ell_s \equiv 2\kappa\xi K(\kappa^2), \quad (51)$$

where $K(\kappa^2)$ is the complete elliptic integral of the first kind. The kinetic and quadratic Zeeman energies are calculated as

$$E_{\text{kin}} = \frac{\hbar^2}{2M} \frac{1}{\xi\ell_s} \frac{E(\kappa^2)}{\kappa}, \quad (52)$$

$$\begin{aligned} E_q &= \frac{1}{L^2} \int d^2r \frac{q}{2} (1 + \hat{f}_z^2) \\ &= \frac{q}{2} - \frac{q\xi}{\ell_s} \frac{E(\kappa^2)}{\kappa}, \end{aligned} \quad (53)$$

where $E(\kappa^2)$ is the complete elliptic integral of the second kind. The domain wall width is estimated to be the length at which the summation of the two energies has a minimum value. Solving $\partial(E_{\text{kin}} + E_q)/\partial\xi = 0$, we obtain

$$\xi = \frac{\hbar}{\sqrt{-2Mq}}. \quad (54)$$

For estimation of ℓ_s , we need to take the MDDI energy into account. For simplicity, we assume $\ell_s \gg \xi$, and take $\hat{f}_x = \hat{f}_y = 0$ and

$$\begin{aligned} \hat{f}_z &= \begin{cases} -1 & \text{for } (2n-1)\ell_s < x < 2n\ell_s \\ 1 & \text{for } 2n\ell_s < x < (2n+1)\ell_s \end{cases} \\ &= \sum_{n=1}^{\infty} \frac{1 - (-1)^n}{in\pi} (e^{in\pi x/\ell_s} - e^{-in\pi x/\ell_s}), \end{aligned} \quad (55)$$

where n is an integer. From Eqs. (33), (37), and (42), we can calculate the MDDI energy as

$$E_{\text{dd}} = -\frac{4\pi}{3} c_{\text{dd}} \tilde{n}_{\text{tot}} \sum_{n=1}^{\infty} [-2 + 3G(n\pi d/\ell_s)] \left[\frac{1 - (-1)^n}{n\pi} \right]^2. \quad (56)$$

Instead of using the original definition of $G(k)$, we use an approximate function $G(k) \simeq 1 - \exp(-\sqrt{\pi}k)$. Then, Eq. (56) is rewritten as

$$E_{\text{dd}} = -\frac{4\pi}{3} c_{\text{dd}} \tilde{n}_{\text{tot}} \left\{ \frac{1}{2} + \frac{6}{\pi^2} \left[\text{Li}_2(-e^{-\pi\sqrt{\pi}d/\ell_s}) - \text{Li}_2(e^{-\pi\sqrt{\pi}d/\ell_s}) \right] \right\}, \quad (57)$$

where $\text{Li}_s(z) \equiv \sum_{k=0}^{\infty} z^k/k^s$ is the polylogarithm. We estimate ℓ_s to be the length at which the total energy has its minimum value in the limit of $\kappa \rightarrow 1$ [thus $E(\kappa^2) \rightarrow 1$]. Solving $\partial(E_{\text{kin}} + E_q + E_{\text{dd}})/\partial\ell_s = 0$ and taking $\kappa = 1$, we obtain

$$\ell_s = \frac{\sqrt{\pi}^3 d}{2} \frac{1}{\text{arctanh} \left[\exp \left(-\frac{\hbar^2/(M\xi)}{8c_{\text{dd}}\tilde{n}_{\text{tot}}\sqrt{\pi}d} \right) \right]}. \quad (58)$$

In Fig. 4(a), we plot the q dependence of ℓ_i , ξ , and ℓ_s for $n_{\text{tot}} = 6n_{\text{tot}}^{(0)}$. The estimated domain size is in good agreement with the average domain size of the simulations; e.g., for $q/h = -40$, the estimated domain size $\ell_s \simeq 24 \mu\text{m}$ from Eq. (58) and the average domain size $\bar{\ell}_s \sim 20 \mu\text{m}$ from simulations shown in Fig. 2(b). The stable domain size ℓ_s is larger than the initial domain size ℓ_i . This property is consistent with the simulations in which initially small magnetic domains appear within a short time before spreading to form a stable (or metastable) pattern. The q dependence of ℓ_s is also consistent with the simulations in which the domain size increases as $|q|$ increases.

The domain size of a stable pattern depends also on the number density. In Fig. 4(b), ℓ_s is plotted for $n_{\text{tot}} = 3n_{\text{tot}}^{(0)}$, $6n_{\text{tot}}^{(0)}$, $10n_{\text{tot}}^{(0)}$ and $20n_{\text{tot}}^{(0)}$. The smaller the value of n_{tot} , the larger the ℓ_s . For the typical number density $n_{\text{tot}} = n_{\text{tot}}^{(0)}$ in experiments [3-5], the estimated domain size is too large to observe in a conventional experimental system.

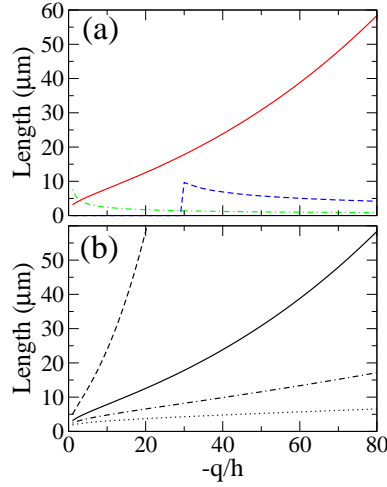


FIG. 4: (Color online) Dependence of theoretical characteristic lengths on $-q/h$ for the hydrodynamic description. (a) Theoretically estimated characteristic lengths of a stripe pattern (solid curve) [Eq. (58)], a pattern at its emergence (dashed curve) [Eq. (49) with Eq. (46)], and the domain wall width (dot-dashed curve) [Eq. (54)] for $n_{\text{tot}} = 6n_{\text{tot}}^{(0)}$. (b) Theoretical characteristic length of a stripe pattern [Eq. (58)] for $n_{\text{tot}} = 3n_{\text{tot}}^{(0)}$ (dashed line), $6n_{\text{tot}}^{(0)}$ (solid line), $10n_{\text{tot}}^{(0)}$ (dot-dashed line), and $20n_{\text{tot}}^{(0)}$ (dotted line).

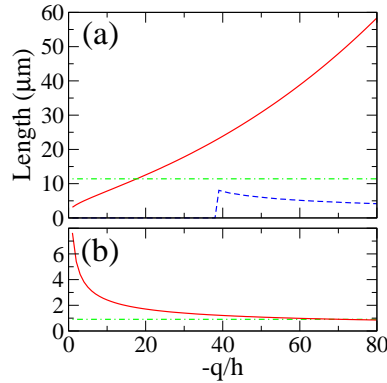


FIG. 5: (Color online) Dependence of theoretical characteristic lengths on $-q/h$ for the GP equation. (a) Theoretically estimated characteristic lengths of the stripe pattern with fully-magnetized domain walls (solid curve) [Eq. (58)], that of the stripe pattern without transverse magnetization (dot-dashed line) [Eq. (65)], and that of a pattern at its emergence (dashed curve) [Eq. (49) with Eq. (47)] for $n_{\text{tot}} = 6n_{\text{tot}}^{(0)}$. (b) Theoretically estimated domain width of the stripe pattern with fully-magnetized domain walls (solid curve) [Eq. (54)] and that of the stripe pattern without transverse magnetization (dot-dashed line) [Eq. (64)] for $n_{\text{tot}} = 6n_{\text{tot}}^{(0)}$.

C. Domain size estimated from the GP equation

In the GP equation, spins are not always fully magnetized. Even when $\hat{f}_z \simeq \pm 1$ over most of a magnetic domain pattern, the magnetization in the domain walls may vanish. The domain wall structure depends on the ferromagnetic interaction ($c_1 n_{\text{tot}}$), which competes with the quadratic Zeeman and kinetic energies. The ferromagnetic interaction lowers energy for high spin density. In other words, the transverse magnetization exists in the domain wall between magnetic domains with $\hat{f}_z \simeq \pm 1$, when the ferromagnetic interaction is strong. On the other hand, the quadratic Zeeman energy prefers a state with sublevels $m = \pm 1$. Here, let us consider two states with $\hat{f}_z = 0$; for instance, (a) $(\zeta_1, \zeta_0, \zeta_{-1})^T = (1/2, 1/\sqrt{2}, 1/2)^T$ and (b) $(1/\sqrt{2}, 0, 1/\sqrt{2})^T$. State (a) corresponds to $\hat{f}_x = 1$ and $\hat{f}_y = \hat{f}_z = 0$ (transverse magnetization), and state (b) to $\hat{f}_x = \hat{f}_y = \hat{f}_z = 0$ (zero magnetization). Comparing them, one can find that the quadratic Zeeman energy of state (b) is smaller than that of state (a). In other words, domain walls with zero magnetization appear when the quadratic Zeeman energy is dominant. Therefore, the domain wall structure changes at around $|c_1| \tilde{n}_{\text{tot}} \simeq |q|$.

Now we estimate characteristic lengths of magnetic domains for $|c_1|\tilde{n}_{\text{tot}} < |q|$. Since zero magnetization is preferred in domain walls, we assume the stripe pattern in this case is described by

$$\psi_1 = \sqrt{\tilde{n}_{\text{tot}}} \cos \frac{\theta - \pi/2}{2}, \quad \psi_0 = 0, \quad \psi_{-1} = \sqrt{\tilde{n}_{\text{tot}}} \sin \frac{\theta - \pi/2}{2}, \quad (59)$$

with $\theta = \text{am}(x/\kappa\xi, \kappa^2)$, where $\text{am}(x/\kappa\xi, \kappa^2)$ is the Jacobi amplitude. Equation (59) corresponds to

$$\hat{f}_x = \hat{f}_y = 0, \quad \hat{f}_z = \text{sn}(x/\kappa\xi, \kappa^2). \quad (60)$$

Then, the kinetic, quadratic Zeeman, and ferromagnetic interaction energies are calculated as

$$E_{\text{kin}} = \frac{\hbar^2}{4M} \frac{1}{\xi\ell_s} \frac{E(\kappa^2)}{\kappa}, \quad (61)$$

$$E_q = q, \quad (62)$$

$$\begin{aligned} E_{c1} &= \frac{c_1\tilde{n}_{\text{tot}}}{2} \frac{1}{L^2} \int dr^2 \hat{\mathbf{f}}^2(\mathbf{r}) \\ &= \frac{c_1\tilde{n}_{\text{tot}}}{2} \left[\frac{1}{\kappa^2} - \frac{2\xi}{\ell_s} \frac{E(\kappa^2)}{\kappa} \right]. \end{aligned} \quad (63)$$

Note that E_q is independent of ξ and ℓ_s . Solving $\partial(E_{\text{kin}} + E_{c1})/\partial\xi = 0$ in the $\kappa \rightarrow 1$ limit, we obtain

$$\xi = \frac{\hbar}{\sqrt{-4Mc_1\tilde{n}_{\text{tot}}}}. \quad (64)$$

In Fig. 5(b), Eq. (64) is plotted as the dot-dashed line, while the solid curve is the plot of Eq. (54). Equation (64) is valid for $|q| > |c_1|\tilde{n}_{\text{tot}} \simeq 35\hbar$. In this region, the values of ξ of both equations almost coincide, as seen in Fig. 5(b).

To estimate the domain size of the stripe pattern, we again assume the MDDI energy is given by Eq. (57). Solving $\partial(E_{\text{kin}} + E_{c1} + E_{\text{dd}})/\partial\ell_s = 0$ with $\kappa = 1$, we obtain

$$\ell_s = \frac{\sqrt{\pi}^3 d}{2} \frac{1}{\text{arctanh} \left[\exp \left(-\frac{\hbar^2/(M\xi)}{16c_{\text{dd}}\tilde{n}_{\text{tot}}\sqrt{\pi}d} \right) \right]}. \quad (65)$$

In Fig. 5(a), Eq. (65) is plotted as the dot-dashed line and compared with the solid curve given by Eq. (58). The dashed curve expresses the domain size ℓ_1 at the beginning of domain pattern formation and has a nonzero value above the threshold. Since $|q| > |c_1|\tilde{n}_{\text{tot}}$ in the region above the threshold, the domain size ℓ_s is estimated by Eq. (65) instead of Eq. (58) for the stable pattern simulated by the GP equation. Also in this case, the estimated domain size is in good agreement with the average domain size obtained from simulations.

VI. CONCLUSIONS AND OUTLOOK

We have derived the dissipative hydrodynamic equation of a ferromagnetic Bose-Einstein condensate (BEC). This equation has the same form as the extended Landau-Lifshitz-Gilbert (LLG) equation, which was originally developed to explain the spin dynamics in a conducting ferromagnet interacting with spin-polarized currents, including an adiabatic spin-transfer torque term. The dissipative hydrodynamic equation enables us to investigate how the domain formation dynamics are affected by the superfluid velocity \mathbf{v}_{mass} , which is inseparable in the Gross-Pitaevskii (GP) equation.

We have demonstrated domain pattern formation simulated by the dissipative hydrodynamic equation with and without \mathbf{v}_{mass} . Although no remarkable difference appears at the beginning of domain pattern formation, \mathbf{v}_{mass} has an effect on later domain formation dynamics: pattern formation is faster in the presence than in the absence of \mathbf{v}_{mass} . We have also shown simulations of the GP equation and compared them with those of the hydrodynamic equation. The dependence on q , which characterizes the quadratic Zeeman energy, of domain pattern formation is different between hydrodynamic and GP simulations because the threshold for a nonuniform magnetic pattern differs between them. Nevertheless, for large $|q|$, magnetic domain patterns eventually come to look similar in both simulations, although they differ in size. The difference is caused by the fact that the assumption of full magnetization for the hydrodynamic description is not satisfied for large $|q|$ in the GP simulations.

To explain the difference in domain size between the hydrodynamic and GP equation simulations, we have estimated the characteristic lengths of the domain patterns. The domain size at the beginning of pattern formation is estimated by means of the linear stability analysis. The difference in domain size for a short time is based on the dynamical instability. The domain size of the domain pattern in the stationary configuration is estimated using the ansatz of the stripe pattern of longitudinal magnetization domains. The analytical estimations are in good agreement with the numerical simulations.

In conclusion, the dissipative hydrodynamic equation provides a simple approach to discuss magnetization dynamics in a ferromagnetic BEC. The hydrodynamic equation simulation qualitatively well reproduces the domain formation dynamics that are simulated by the GP equation. However, quantitative discrepancies arise when the assumption of the hydrodynamic description fails: for instance, the ferromagnetic interaction energy becomes comparable with the quadratic Zeeman energy. The analogy between the dissipative hydrodynamic equation and the extended LLG equation can provide suggestions on new experiments of a ferromagnetic BEC to investigate interesting phenomena that are observed in conducting ferromagnets.

One of such interesting and possible phenomena is the anomalous Hall effect (AHE), which is the Hall effect due to the magnetization and observed in conducting ferromagnets. Here, we focus on the AHE caused by a skyrmion configuration or spin chirality [24–27], although there are several mechanisms to cause the phenomenon. The Berry phase, which is generated by a skyrmion configuration, induces an effective magnetic field or gauge flux. When an electric field is applied, electrons move to the perpendicular direction to both the electric and the effective magnetic field. This is the mechanism of the AHE due to spin chirality. Inversely, the electric current can move the skyrmion. The AHE is expected to be observed very clearly in the adiabatic limit, where a ferromagnetic BEC is supposed to realize. Unfortunately, there are difficulties for observation of the AHE in a ferromagnetic BEC: for example, it is difficult to create the external field that corresponds to the electric field of a conducting ferromagnet system. However, the essential aspect of the AHE (i.e., the interaction between current and spin chirality) can be investigated in a ferromagnetic BEC. Experimentally, one can create a current by sudden change of a trapping potential or the fictitious field that is created through the vector potential induced by a laser field [38]. The investigation about the interaction between current and spin configuration in a ferromagnetic BEC will give an insight on pure adiabatic spin-transfer effects.

Acknowledgments

The authors thank M. Ueda for his useful comments. This work is supported by MEXT JSPS KAKENHI (No. 22103005, 22340114, 22740265), the Photon Frontier Network Program of MEXT, Japan, Hayashi Memorial Foundation for Female Natural Scientists, and JSPS and FRST under the Japan-New Zealand Research Cooperative Program.

Appendix A: Time evolution of \mathbf{v}_{mass}

Substituting Eq. (18) into Eq. (14) and applying Ψ_m^* from the left, we have

$$\begin{aligned} & (i - \Gamma)\hbar \left(\sqrt{n_{\text{tot}}} \frac{\partial \sqrt{n_{\text{tot}}}}{\partial t} + in_{\text{tot}} \frac{\partial \phi'}{\partial t} - in_{\text{tot}} F \cos \beta \frac{\partial \alpha}{\partial t} \right) \\ &= -\frac{\hbar^2}{2M} \Psi_m^{(0)*} \{ [\nabla + i\nabla\phi' - i(\nabla\alpha)e^{iF_y\beta} F_z e^{-iF_y\beta} - i(\nabla\beta)F_y]^2 \}_{mn} \Psi_n^{(0)} \\ &+ \Psi_m^* H_{mn} \Psi_n - n_{\text{tot}} \mu(t), \end{aligned} \quad (\text{A1})$$

where we have used $\Psi_m = e^{i\phi'} U_{mn} \Psi_n^{(0)}$. The first term on the right hand side is calculated as

$$\begin{aligned} & \Psi_m^{(0)*} \{ [\nabla + i\nabla\phi' - i(\nabla\alpha)e^{iF_y\beta} F_z e^{-iF_y\beta} - i(\nabla\beta)F_y]^2 \}_{mn} \Psi_n^{(0)} \\ &= n_{\text{tot}} \zeta_m^{(0)*} \left\{ \frac{\nabla^2 \sqrt{n_{\text{tot}}}}{\sqrt{n_{\text{tot}}}} - [\nabla\phi' - F_z(\nabla\alpha) \cos \beta]^2 - [F_x(\nabla\alpha) \sin \beta - F_y(\nabla\beta)]^2 \right\}_{mn} \zeta_n^{(0)} \\ &+ i\zeta_m^{(0)*} \{ n_{\text{tot}} \nabla \cdot [\nabla\phi' - F_z(\nabla\alpha) \cos \beta] + 2\sqrt{n_{\text{tot}}} \nabla \sqrt{n_{\text{tot}}} \cdot [\nabla\phi' - F_z(\nabla\alpha) \cos \beta] \}_{mn} \zeta_n^{(0)} \\ &= n_{\text{tot}} \left[\frac{\nabla^2 \sqrt{n_{\text{tot}}}}{\sqrt{n_{\text{tot}}}} - \left(\frac{M}{\hbar} \mathbf{v}_{\text{mass}} \right)^2 - \frac{F}{2} (\nabla \hat{\mathbf{f}})^2 \right] + i \frac{M}{\hbar} \nabla \cdot (n_{\text{tot}} \mathbf{v}_{\text{mass}}), \end{aligned} \quad (\text{A2})$$

where we have used Eq. (23) and the following equations:

$$\zeta_m^{(0)*} (F_\mu)_{mn} \zeta_n^{(0)} = F \delta_{\mu z}, \quad (\text{A3})$$

$$e^{iF_y \beta} F_z e^{-iF_y \beta} = F_z \cos \beta - F_x \sin \beta, \quad (\text{A4})$$

$$\begin{aligned} \zeta_m^{(0)*} \left\{ [F_x (\nabla \alpha) \sin \beta - F_y (\nabla \beta)]^2 \right\}_{mn} \zeta_n^{(0)} &= \frac{F}{2} [(\nabla \alpha)^2 \sin^2 \beta + (\nabla \beta)^2] \\ &= \frac{F}{2} (\nabla \hat{\mathbf{f}})^2. \end{aligned} \quad (\text{A5})$$

The imaginary part of Eq. (A1) reads

$$\frac{\partial n_{\text{tot}}}{\partial t} = 2\Gamma n_{\text{tot}} \left(\frac{\partial \phi'}{\partial t} - F \cos \beta \frac{\partial \alpha}{\partial t} \right) - \nabla \cdot (n_{\text{tot}} \mathbf{v}_{\text{mass}}). \quad (\text{A6})$$

From the real part of Eq. (A1), we have

$$\frac{\hbar \Gamma}{2n_{\text{tot}}} \frac{\partial n_{\text{tot}}}{\partial t} + \hbar \left(\frac{\partial \phi'}{\partial t} - F \cos \beta \frac{\partial \alpha}{\partial t} \right) + [\mu_{\text{local}} - \mu(t)] = 0, \quad (\text{A7})$$

where

$$\mu_{\text{local}}(\mathbf{r}, t) = \frac{\Psi_m^* H_{mn} \Psi_n}{n_{\text{tot}}} - \frac{\hbar^2}{2M} \frac{\nabla^2 \sqrt{n_{\text{tot}}}}{\sqrt{n_{\text{tot}}}} + \frac{M}{2} \mathbf{v}_{\text{mass}}^2 + \frac{\hbar^2 F}{4M} (\nabla \hat{\mathbf{f}})^2. \quad (\text{A8})$$

Combining Eqs. (A6) and (A7) and eliminating $(\partial \phi' / \partial t - F \cos \beta \partial \alpha / \partial t)$, we obtain Eq. (25) as follows:

$$\frac{\partial n_{\text{tot}}}{\partial t} = -\frac{1}{1 + \Gamma^2} \nabla \cdot (n_{\text{tot}} \mathbf{v}_{\text{mass}}) - \frac{\Gamma}{1 + \Gamma^2} \frac{2}{\hbar} n_{\text{tot}} [\mu_{\text{local}} - \mu(t)]. \quad (\text{A9})$$

On the other hand, substituting Eq. (A6) into Eq. (A9), we have

$$\hbar \left(\frac{\partial \phi'}{\partial t} - F \cos \beta \frac{\partial \alpha}{\partial t} \right) = -\frac{1}{1 + \Gamma^2} [\mu_{\text{local}} - \mu(t)] + \frac{\Gamma}{1 + \Gamma^2} \frac{\hbar}{2n_{\text{tot}}} \nabla \cdot (n_{\text{tot}} \mathbf{v}_{\text{mass}}). \quad (\text{A10})$$

The gradient of the left hand side of Eq. (A10) is

$$\begin{aligned} \hbar \nabla \left(\frac{\partial \phi'}{\partial t} - F \cos \beta \frac{\partial \alpha}{\partial t} \right) &= \hbar \left\{ \frac{\partial}{\partial t} [\nabla \phi' - F (\nabla \alpha) \cos \beta] - F \left[(\nabla \cos \beta) \frac{\partial \alpha}{\partial t} - (\nabla \alpha) \frac{\partial \cos \beta}{\partial t} \right] \right\} \\ &= M \frac{\partial}{\partial t} \mathbf{v}_{\text{mass}} - \hbar F \left[(\nabla \alpha) \sin \beta \frac{\partial \beta}{\partial t} - (\nabla \beta) \sin \beta \frac{\partial \alpha}{\partial t} \right]. \end{aligned} \quad (\text{A11})$$

Here, we introduce vectors $\hat{\mathbf{m}}$ and $\hat{\mathbf{n}}$, which are orthogonal to $\hat{\mathbf{f}}$,

$$\hat{\mathbf{f}} = \begin{pmatrix} \sin \beta \cos \alpha \\ \sin \beta \sin \alpha \\ \cos \beta \end{pmatrix}, \quad \hat{\mathbf{m}} = \begin{pmatrix} \cos \beta \cos \alpha \\ \cos \beta \sin \alpha \\ -\sin \beta \end{pmatrix}, \quad \hat{\mathbf{n}} = \begin{pmatrix} -\sin \alpha \\ \cos \alpha \\ 0 \end{pmatrix}. \quad (\text{A12})$$

One can easily see

$$\hat{\mathbf{m}} = \hat{\mathbf{n}} \times \hat{\mathbf{f}}, \quad \hat{\mathbf{n}} = \hat{\mathbf{f}} \times \hat{\mathbf{m}} \quad (\text{A13})$$

$$\partial \hat{\mathbf{f}} = (\partial \beta) \hat{\mathbf{m}} + (\partial \alpha) \sin \beta \hat{\mathbf{n}}. \quad (\text{A14})$$

Employing these vectors, we have

$$\begin{aligned} (\nabla \hat{\mathbf{f}}) \cdot \left(\hat{\mathbf{f}} \times \frac{\partial \hat{\mathbf{f}}}{\partial t} \right) &= [(\nabla \beta) \hat{\mathbf{m}} + (\nabla \alpha) \sin \beta \hat{\mathbf{n}}] \cdot \left[\hat{\mathbf{f}} \times \left(\frac{\partial \beta}{\partial t} \hat{\mathbf{m}} + \frac{\partial \alpha}{\partial t} \sin \beta \hat{\mathbf{n}} \right) \right] \\ &= [(\nabla \beta) \hat{\mathbf{m}} + (\nabla \alpha) \sin \beta \hat{\mathbf{n}}] \cdot \left(\frac{\partial \beta}{\partial t} \hat{\mathbf{n}} - \frac{\partial \alpha}{\partial t} \sin \beta \hat{\mathbf{m}} \right) \\ &= (\nabla \alpha) \sin \beta \frac{\partial \beta}{\partial t} - (\nabla \beta) \sin \beta \frac{\partial \alpha}{\partial t}. \end{aligned} \quad (\text{A15})$$

From Eqs.(A10), (A11) and (A15), we obtain Eq. (27) as follows:

$$M \frac{\partial}{\partial t} \mathbf{v}_{\text{mass}} = -\nabla \left[\frac{\mu_{\text{local}} - \mu(t)}{1 + \Gamma^2} - \frac{\Gamma}{1 + \Gamma^2} \frac{\hbar}{2n_{\text{tot}}} \nabla \cdot (n_{\text{tot}} \mathbf{v}_{\text{mass}}) \right] + \hbar F (\nabla \hat{\mathbf{f}}) \cdot \left(\hat{\mathbf{f}} \times \frac{\partial \hat{\mathbf{f}}}{\partial t} \right). \quad (\text{A16})$$

Appendix B: Time evolution of \mathbf{f}

The time evolution of the normalized spin density is calculated as

$$\begin{aligned}
\frac{\partial \hat{f}_\mu}{\partial t} &= \frac{1}{Fn_{\text{tot}}} \left[\Psi_m^*(F_\mu)_{mn} \frac{\partial \Psi_n}{\partial t} + \frac{\partial \Psi_m^*}{\partial t} (F_\mu)_{mn} \Psi_n \right] - \frac{\partial n_{\text{tot}}}{\partial t} \frac{\hat{f}_\mu}{n_{\text{tot}}} \\
&= \frac{1}{Fn_{\text{tot}}} \frac{1}{\hbar(1+\Gamma^2)} \left\{ -\frac{\hbar^2}{2M} [(-i-\Gamma)\Psi_m^*(F_\mu)_{mn} \nabla^2 \Psi_n + (i-\Gamma)(\nabla^2 \Psi_m^*)(F_\mu)_{mn} \Psi_n] \right. \\
&\quad \left. + (-i-\Gamma)\Psi_m^*(F_\mu)_{ml} [H - \mu(t)]_{ln} \Psi_n + (i-\Gamma)\Psi_m^* [H - \mu(t)]_{ml} (F_\mu)_{ln} \Psi_n \right\} \\
&= \frac{1}{Fn_{\text{tot}}} \frac{1}{\hbar(1+\Gamma^2)} \left\{ -\frac{\hbar^2}{M} [\text{Im}(\Psi_m^*(F_\mu)_{mn} \nabla^2 \Psi_n) - \Gamma \text{Re}(\Psi_m^*(F_\mu)_{mn} \nabla^2 \Psi_n)] \right. \\
&\quad \left. + 2 [\text{Im}(\Psi_m^*(F_\mu)_{ml} H_{ln} \Psi_n) - \Gamma \text{Re}(\Psi_m^*(F_\mu)_{ml} H_{ln} \Psi_n)] + 2\Gamma\mu(t) \right\}, \tag{B1}
\end{aligned}$$

where we have assumed $\partial n_{\text{tot}}/\partial t = 0$.

1. Kinetic energy terms

First, we calculate the spacial derivative terms. Making use of Eqs. (A4) and (A12), we have

$$\begin{aligned}
\Psi_m^*(F_\mu)_{mn} \nabla^2 \Psi_n &= \zeta_m^{(0)*} (F_x \hat{m}_\mu + F_y \hat{n}_\mu + F_z \hat{f}_\mu) \left\{ \sqrt{n_{\text{tot}}} \nabla^2 \sqrt{n_{\text{tot}}} \right. \\
&\quad \left. + i n_{\text{tot}} \nabla \cdot [\nabla \phi' - (\nabla \alpha) F_z \cos \beta + (\nabla \alpha) F_x \sin \beta - (\nabla \beta) F_y] \right. \\
&\quad \left. + i \nabla n_{\text{tot}} \cdot [\nabla \phi' - (\nabla \alpha) F_z \cos \beta + (\nabla \alpha) F_x \sin \beta - (\nabla \beta) F_y] \right. \\
&\quad \left. - n_{\text{tot}} [\nabla \phi' - (\nabla \alpha) F_z \cos \beta + (\nabla \alpha) F_x \sin \beta - (\nabla \beta) F_y]^2 \right\}_{mn} \zeta_n^{(0)}. \tag{B2}
\end{aligned}$$

Using Eqs. (23), (A5), (A13), (A14) and the relation

$$(\nabla \alpha) \sin \beta \hat{\mathbf{m}} - (\nabla \beta) \hat{\mathbf{n}} = -\hat{\mathbf{f}} \times \nabla \hat{\mathbf{f}}, \tag{B3}$$

$$(\nabla \alpha) \sin \beta \hat{\mathbf{n}} + (\nabla \beta) \hat{\mathbf{m}} = -\hat{\mathbf{f}} \times (\hat{\mathbf{f}} \times \nabla \hat{\mathbf{f}}), \tag{B4}$$

we obtain

$$\begin{aligned}
\frac{\Psi_m^*(F_\mu)_{mn} \nabla^2 \Psi_n}{Fn_{\text{tot}}} &= - \left\{ -\frac{\nabla^2 \sqrt{n_{\text{tot}}}}{\sqrt{n_{\text{tot}}}} + \left(\frac{M}{\hbar} \mathbf{v}_{\text{mass}} \right)^2 + \frac{F}{2} (\nabla \hat{\mathbf{f}})^2 \right\} \hat{f}_\mu + \frac{M}{\hbar} \left[\hat{\mathbf{f}} \times (\mathbf{v}_{\text{mass}} \cdot \nabla) \hat{\mathbf{f}} \right]_\mu \\
&\quad - \frac{1}{2} \left[\hat{\mathbf{f}} \times (\hat{\mathbf{f}} \times \nabla^2 \hat{\mathbf{f}}) \right]_\mu - \frac{1}{2} \left[\hat{\mathbf{f}} \times \left(\hat{\mathbf{f}} \times \frac{\nabla n_{\text{tot}}}{n_{\text{tot}}} \cdot \nabla \hat{\mathbf{f}} \right) \right]_\mu \\
&\quad + i \frac{M}{\hbar} \left[\frac{\nabla \cdot (n_{\text{tot}} \mathbf{v}_{\text{mass}})}{n_{\text{tot}}} \hat{f}_\mu + (\mathbf{v}_{\text{mass}} \cdot \nabla) \hat{f}_\mu \right] \\
&\quad - \frac{i}{2} \left[\hat{\mathbf{f}} \times \nabla^2 \hat{\mathbf{f}} \right]_\mu - \frac{i}{2} \left[\hat{\mathbf{f}} \times \frac{\nabla n_{\text{tot}}}{n_{\text{tot}}} \cdot \nabla \hat{\mathbf{f}} \right]_\mu. \tag{B5}
\end{aligned}$$

From this equation and Eq. (28), we can rewrite the space derivative terms of Eq. (B1) as

$$\begin{aligned}
\text{Re} \left[\frac{\Psi_m^*(F_\mu)_{mn} \nabla^2 \Psi_n}{Fn_{\text{tot}}} \right] &= \frac{2M}{\hbar^2} \left(\frac{\Psi_m^* H_{mn} \Psi_n}{n_{\text{tot}}} - \mu_{\text{local}} \right) \hat{f}_\mu \\
&\quad + \left\{ \hat{\mathbf{f}} \times \left[\frac{M}{\hbar} (\mathbf{v}_{\text{mass}} \cdot \nabla) \hat{\mathbf{f}} - \frac{1}{2} \hat{\mathbf{f}} \times (\nabla^2 \hat{\mathbf{f}} + (\mathbf{a} \cdot \nabla) \hat{\mathbf{f}}) \right] \right\}_\mu, \tag{B6}
\end{aligned}$$

$$\text{Im} \left[\frac{\Psi_m^*(F_\mu)_{mn} \nabla^2 \Psi_n}{Fn_{\text{tot}}} \right] = -\Gamma \frac{2M}{\hbar^2} [\mu_{\text{local}} - \mu(t)] \hat{f}_\mu + \left[\frac{M}{\hbar} (\mathbf{v}_{\text{mass}} \cdot \nabla) \hat{\mathbf{f}} - \frac{1}{2} \hat{\mathbf{f}} \times (\nabla^2 \hat{\mathbf{f}} + (\mathbf{a} \cdot \nabla) \hat{\mathbf{f}}) \right]_\mu, \tag{B7}$$

where $\mathbf{a} = \nabla n_{\text{tot}}/n_{\text{tot}}$.

2. Short-range interaction terms

Next, we calculate the contributions of the short-range interaction $\Psi_m^*(F_\mu)_{ml}H_{ln}^s\Psi_n$, where

$$H_{mn}^s = C_{nn'}^{mm'}\Psi_{m'}^*\Psi_{n'}, \quad (\text{B8})$$

$$C_{nn'}^{mm'} \equiv \sum_{S=0} \frac{4\pi\hbar^2}{M} a_S \langle Fm, Fm' | \mathcal{P}_S | Fn', Fn \rangle. \quad (\text{B9})$$

Now we rewrite the matrix elements of the short-range interaction $C_{nn'}^{mm'}$ in terms of the spin matrices. The projection operator \mathcal{P}_S satisfies the completeness relation $\sum_S \mathcal{P}_S = 1$, that is,

$$\delta_{mn}\delta_{m'n'} = \sum_{S=0, \text{even}}^{2F} \langle Fm, Fm' | \mathcal{P}_S | Fn', Fn \rangle. \quad (\text{B10})$$

On the other hand, from the identity equation

$$(\mathbf{F}_1 \cdot \mathbf{F}_2)^k = \left[\frac{(\mathbf{F}_1 + \mathbf{F}_2)^2 - \mathbf{F}_1^2 - \mathbf{F}_2^2}{2} \right]^k, \quad (\text{B11})$$

we obtain

$$\begin{aligned} & (F_{\nu_1} F_{\nu_2} \cdots F_{\nu_k})_{mn} (F_{\nu_1} F_{\nu_2} \cdots F_{\nu_k})_{m'n'} \\ &= \sum_{S=0, \text{even}}^{2F} \left[\frac{S(S+1) - 2F(F+1)}{2} \right]^k \langle Fm, Fm' | \mathcal{P}_S | Fn', Fn \rangle. \end{aligned} \quad (\text{B12})$$

Using Eqs. (B10) and (B12), $C_{nn'}^{mm'}$ can be generally expressed as

$$C_{nn'}^{mm'} = \Lambda_0 \delta_{mn} \delta_{m'n'} + \sum_{k=1}^F \Lambda_k (F_{\nu_1} F_{\nu_2} \cdots F_{\nu_k})_{mn} (F_{\nu_1} F_{\nu_2} \cdots F_{\nu_k})_{m'n'}, \quad (\text{B13})$$

where Λ_0 and Λ_k are given by the linear combinations of a_S . For the case of $F = 1$, for example, we obtain $\Lambda_0 = c_0 = \pi\hbar^2(2a_2 + a_0)/(3M)$ and $\Lambda_1 = c_1 = 4\pi\hbar^2(a_0 - a_2)/(3M)$, and $C_{nn'}^{mm'}$ can be written in the following form:

$$C_{nn'}^{mm'} = c_0 \delta_{mn} \delta_{m'n'} + c_1 (\mathbf{F})_{mn} \cdot (\mathbf{F})_{m'n'}. \quad (\text{B14})$$

Substituting Eq. (B13) to Eq. (B8), we obtain

$$H_{mn}^s = C_{nn'}^{mm'} \Psi_{m'}^* \Psi_{n'} \quad (\text{B15})$$

$$= \Lambda_0 n_{\text{tot}} \delta_{mn} + \sum_{k=1}^F \Lambda_k n_{\text{tot}} \mathcal{M}_{\nu_1 \nu_2 \cdots \nu_k} (F_{\nu_1} F_{\nu_2} \cdots F_{\nu_k})_{mn}, \quad (\text{B16})$$

where

$$\mathcal{M}_{\nu_1 \nu_2 \cdots \nu_k} = \zeta_m^* (F_{\nu_1} F_{\nu_2} \cdots F_{\nu_k})_{mn} \zeta_n, \quad (\text{B17})$$

and we have used $\Psi_m = \sqrt{n_{\text{tot}}} \zeta_m$ and $\zeta_m^* \zeta_m = 1$.

When we consider the ferromagnetic state (i.e., when the order parameter is given by $\Psi_m = \sqrt{n_{\text{tot}}} e^{i\phi'} U_{mn} \zeta_n^{(0)}$ with $\zeta_m^{(0)} = \delta_{mF}$), we have

$$\begin{aligned} \mathcal{M}_{\nu_1 \nu_2 \cdots \nu_k} &= \zeta_m^{(0)*} (U^\dagger F_{\nu_1} U U^\dagger F_{\nu_2} U \cdots U^\dagger F_{\nu_k} U)_{mn} \zeta_n^{(0)} \\ &= \mathcal{R}_{\nu_1 \nu_1'} \mathcal{R}_{\nu_2 \nu_2'} \cdots \mathcal{R}_{\nu_k \nu_k'} (F_{\nu_1'} F_{\nu_2'} \cdots F_{\nu_k'})_{FF} \\ &= \mathcal{R}_{\nu_1 \nu_1'} \mathcal{R}_{\nu_2 \nu_2'} \cdots \mathcal{R}_{\nu_k \nu_k'} \mathcal{M}_{\nu_1' \nu_2' \cdots \nu_k'}^{(0)}, \end{aligned} \quad (\text{B18})$$

where $\mathcal{M}_{\nu_1\nu_2\cdots\nu_k}^{(0)} \equiv (F_{\nu_1}F_{\nu_2}\cdots F_{\nu_k})_{FF}$, and \mathcal{R} is defined in Eq.(20). Then, $\Psi_m^* H_{mn}^s \Psi_n$ is shown to be independent of the local spin direction:

$$\Psi_m^* H_{mn}^s \Psi_n = n_{\text{tot}}^2 \Lambda_0 + n_{\text{tot}}^2 \sum_{k=1}^F \Lambda_k \mathcal{M}_{\nu_1\nu_2\cdots\nu_k}^{(0)} \mathcal{M}_{\nu_1\nu_2\cdots\nu_k}^{(0)}. \quad (\text{B19})$$

In a similar manner, we obtain

$$\Psi_m^* (F_\mu H^s)_{mn} \Psi_n = n_{\text{tot}}^2 \Lambda_0 F \hat{f}_\mu + n_{\text{tot}}^2 \sum_{k=1}^F \Lambda_k \mathcal{R}_{\mu\mu'} \mathcal{M}_{\nu_1\nu_2\cdots\nu_k}^{(0)} \mathcal{M}_{\mu'\nu_1\nu_2\cdots\nu_k}^{(0)}. \quad (\text{B20})$$

Note here that F_x or F_y has to appear an even number of times in the product of $F_{\nu_1}F_{\nu_2}\cdots F_{\nu_k}$ so that $\mathcal{M}_{\nu_1\nu_2\cdots\nu_k}^{(0)} = (F_{\nu_1}F_{\nu_2}\cdots F_{\nu_k})_{FF}$ is nonzero. Hence, $\mathcal{M}_{\nu_1\nu_2\cdots\nu_k}^{(0)} \mathcal{M}_{\mu'\nu_1\nu_2\cdots\nu_k}^{(0)}$ becomes nonzero only when $\mu' = z$:

$$\mathcal{M}_{\nu_1\nu_2\cdots\nu_k}^{(0)} \mathcal{M}_{\mu'\nu_1\nu_2\cdots\nu_k}^{(0)} = \delta_{\mu'z} F \mathcal{M}_{\nu_1\nu_2\cdots\nu_k}^{(0)} \mathcal{M}_{\nu_1\nu_2\cdots\nu_k}^{(0)}. \quad (\text{B21})$$

Then, Eq. (B20) is written as

$$\begin{aligned} & \Psi_m^* (F_\mu H^s)_{mn} \Psi_n \\ &= n_{\text{tot}}^2 \Lambda_0 F \hat{f}_\mu + n_{\text{tot}}^2 F \mathcal{R}_{\mu z} \sum_{k=1}^F \Lambda_k \mathcal{M}_{\nu_1\nu_2\cdots\nu_k}^{(0)} \mathcal{M}_{\nu_1\nu_2\cdots\nu_k}^{(0)} \end{aligned} \quad (\text{B22})$$

$$= (\Psi_m^* H_{mn}^s \Psi_n) F \hat{f}_\mu. \quad (\text{B23})$$

Thus, we obtain

$$\text{Re}[\Psi_m^* (F_\mu H^s)_{mn} \Psi_n] = (\Psi_m^* H_{mn}^s \Psi_n) F \hat{f}_\mu, \quad (\text{B24})$$

$$\text{Im}[\Psi_m^* (F_\mu H^s)_{mn} \Psi_n] = 0. \quad (\text{B25})$$

3. Other terms

Finally, we calculate the remaining terms. Using Eqs. (15) and (B25), we easily obtain

$$\begin{aligned} \text{Im} \left[\frac{\Psi_m^* (F_\mu)_{ml} H_{ln} \Psi_n}{F n_{\text{tot}}} \right] &= \frac{1}{2i F n_{\text{tot}}} \Psi_m^* [F_\mu, H]_{mn} \Psi_n \\ &= \frac{1}{2i F n_{\text{tot}}} \Psi_m^* \{p[F_\mu, F_z] + q[F_\mu, F_z^2] + c_{\text{dd}} b_\nu [F_\mu, F_\nu]\}_{mn} \Psi_n \\ &= -\frac{1}{2} \left[\hat{\mathbf{f}} \times \left(p \hat{z} + q(2F-1) \hat{f}_z \hat{z} + c_{\text{dd}} \mathbf{b} \right) \right]_\mu. \end{aligned} \quad (\text{B26})$$

Employing Eqs. (15), (B24), and (B25), we obtain

$$\begin{aligned} \text{Re} \left[\frac{\Psi_m^* (F_\mu)_{ml} H_{ln} \Psi_n}{F n_{\text{tot}}} \right] &= \frac{\Psi_m^* H_{mn}^s \Psi_n}{n_{\text{tot}}} \hat{f}_\mu + U_{\text{trap}} \hat{f}_\mu + \frac{p}{2} \left[\delta_{\mu z} + (2F-1) \hat{f}_z \hat{f}_\mu \right] \\ &\quad + \frac{q}{2} \left[(2F^2 - 3F + 1) \hat{f}_z^2 \hat{f}_\mu + F \hat{f}_\mu + (2F-1) \hat{f}_z \delta_{\mu z} \right] \\ &\quad + \frac{c_{\text{dd}}}{2} \left[b_\mu + (2F-1) (\mathbf{b} \cdot \hat{\mathbf{f}}) \hat{f}_\mu \right], \end{aligned} \quad (\text{B27})$$

where we have used

$$\Psi_m^* (F_\mu F_\nu + F_\nu F_\mu)_{mn} \Psi_n = F n_{\text{tot}} \delta_{\mu\nu} + F(2F-1) n_{\text{tot}} \hat{f}_\mu \hat{f}_\nu, \quad (\text{B28})$$

$$\Psi_m^* (F_z^2 F_\mu + F_\mu F_z^2)_{mn} \Psi_n = F n_{\text{tot}} \left[(2F-1) \hat{f}_z \delta_{\mu z} + (2F^2 - 3F + 1) \hat{f}_z^2 \hat{f}_\mu + F \hat{f}_\mu \right]. \quad (\text{B29})$$

Equation (B28) is rewritten as

$$\begin{aligned} \text{Re} \left[\frac{\Psi_m^* (F_\mu)_{ml} H_{ln} \Psi_n}{F n_{\text{tot}}} \right] &= \frac{\Psi_m^* H_{mn} \Psi_n}{n_{\text{tot}}} \hat{f}_\mu + \frac{1}{2} \left[p \hat{z} + q(2F - 1) \hat{f}_z \hat{z} + c_{\text{dd}} \mathbf{b} \right]_\mu \\ &\quad - \frac{1}{2} \left\{ \hat{\mathbf{f}} \cdot \left[p \hat{z} + q(2F - 1) \hat{f}_z \hat{z} + c_{\text{dd}} \mathbf{b} \right] \right\}_\mu \\ &= \frac{\Psi_m^* H_{mn} \Psi_n}{n_{\text{tot}}} \hat{f}_\mu - \frac{1}{2} \left\{ \hat{\mathbf{f}} \times \left[\hat{\mathbf{f}} \times \left(p \hat{z} + q(2F - 1) \hat{f}_z \hat{z} + c_{\text{dd}} \mathbf{b} \right) \right] \right\}_\mu, \end{aligned} \quad (\text{B31})$$

where

$$\Psi_m^* H_{mn} \Psi_n = \Psi_m^* H_{mn}^s \Psi_n + n_{\text{tot}} \left\{ U_{\text{trap}} + pF \hat{f}_z + \frac{q}{2} F \left[1 + 2(F - 1) \hat{f}_z^2 \right] + c_{\text{dd}} F \mathbf{b} \cdot \hat{\mathbf{f}} \right\}. \quad (\text{B32})$$

Substituting Eqs. (B6), (B7), (B27), and (B31) into Eq. (B1), we obtain Eqs. (30) and (31) as follows:

$$\frac{\partial \hat{\mathbf{f}}}{\partial t} = \frac{1}{1 + \Gamma^2} \left[\frac{1}{\hbar} \hat{\mathbf{f}} \times \mathbf{B}_{\text{eff}} - (\mathbf{v}_{\text{mass}} \cdot \nabla) \hat{\mathbf{f}} \right] - \frac{\Gamma}{1 + \Gamma^2} \hat{\mathbf{f}} \times \left[\frac{1}{\hbar} \hat{\mathbf{f}} \times \mathbf{B}_{\text{eff}} - (\mathbf{v}_{\text{mass}} \cdot \nabla) \hat{\mathbf{f}} \right], \quad (\text{B33})$$

$$\mathbf{B}_{\text{eff}} = \frac{\hbar^2}{2M} \nabla^2 \hat{\mathbf{f}} + \frac{\hbar^2}{2M} (\mathbf{a} \cdot \nabla) \hat{\mathbf{f}} - c_{\text{dd}} \mathbf{b} - p \hat{z} - q(2F - 1) \hat{f}_z \hat{z}. \quad (\text{B34})$$

-
- [1] A. J. Leggett, Rev. Mod. Phys. **47**, 331 (1975).
[2] A. S. Borovik-Romanov, Y. M. Bunkov, V. V. Dmitriev, Y.M. Mukharskiy, D.A. Sergatskov, Phys. Rev. Lett. **62**, 1631 (1989).
[3] L. E. Sadler, J. M. Higbie, S. R. Leslie, M. Vengalattore, and D. M. Stamper-Kurn, Nature **443**, 312 (2006).
[4] M. Vengalattore, S. R. Leslie, J. Guzman, and D. M. Stamper-Kurn, Phys. Rev. Lett. **100**, 170403 (2008).
[5] M. Vengalattore, J. Guzman, S. R. Leslie, F. Serwane, and D. M. Stamper-Kurn, Phys. Rev. A **81**, 053612 (2010).
[6] A. Lamacraft, Phys. Rev. A **77**, 063622 (2008).
[7] K. Kudo and Y. Kawaguchi, Phys. Rev. A **82**, 053614 (2010).
[8] R. Barnett, D. Podolsky, and G. Refael, Phys. Rev. B **80**, 024420 (2009).
[9] R. W. Cherng and E. Demler, Phys. Rev. A **83**, 053613 (2011); R. W. Cherng and E. Demler, Phys. Rev. A **83**, 053614 (2011).
[10] J. C. Slonczewski, J. Magn. Magn. Mater. **159**, L1 (1996); L. Berger, Phys. Rev. B **54**, 9353 (1996).
[11] Ya. B. Bazaliy, B. A. Jones, and S.-C. Zhang, Phys. Rev. B **57**, R3213 (1998); Z. Li and S. Zhang, Phys. Rev. Lett. **92**, 207203 (2004).
[12] T.-L. Ho and V. B. Shenoy, Phys. Rev. Lett. **77**, 2595 (1996).
[13] M. Nakahara, T. Isoshima, K. Machida, S. Ogawa, and T. Ohmi, Physica B: Condensed Matter **284–288**, 17 (2000); T. Isoshima, M. Nakahara, T. Ohmi, and K. Machida, Phys. Rev. A **61**, 063610 (2000).
[14] N.D. Mermin and T.-L. Ho, Phys. Rev. Lett. **36**, 594 (1976).
[15] M. Lakshmanan, Phil. Trans. R. Soc. A **369**, 1280-1300 (2011).
[16] G. Tataru, H. Kohno, and J. Shibata, Phys. Rep. **468**, 213 (2008).
[17] S. Zhang and Z. Li, Phys. Rev. Lett. **93**, 127204 (2004); A. Thiaville, Y. Nakatani, J. Miltat, and Y. Suzuki, Europhys. Lett. **69**, 990 (2005).
[18] C.H. Wong and Y. Tserkovnyak, Phys. Rev. B **80**, 184411 (2009).
[19] H. Kohno, G. Tataru, and J. Shibata, J. Phys. Soc. Jpn. **75**, 113706 (2006); Y. Tserkovnyak, H.J. Skadsem, A. Brataas, G.E.W. Bauer, Phys. Rev. B **74**, 144405 (2006).
[20] S. E. Barnes and S. Maekawa, Phys. Rev. Lett. **95**, 107204 (2005); J. He, Z. Li, and S. Zhang, Phys. Rev. B **73**, 184408 (2006).
[21] J. Shibata, Y. Nakatani, G. Tataru, H. Kohno, and Y. Otani, Phys. Rev. B **73**, 020403(R) (2006).
[22] A. Yamaguchi, et al., Phys. Rev. Lett. **92**, 077205 (2004); *ibid.* **96**, 179904(E) (2006); M. Kläui et al., Phys. Rev. Lett. **95**, 026601 (2005).
[23] L. Heyne *et al.*, Phys. Rev. Lett. **105**, 187203 (2010).
[24] J. Ye, Y. B. Kim, A. J. Millis, B. I. Shraiman, P. Majumdar, and Z. Tešanović, Phys. Rev. Lett. **83**, 3737 (1999).
[25] S. Onoda and N. Nagaosa, Phys. Rev. Lett. **90**, 196602 (2003).
[26] M. Onoda, G. Tataru, and N. Nagaosa, J. Phys. Soc. Jpn. **73**, 2624 (2004).
[27] K. Taguchi and G. Tataru, Phys. Rev. B **79**, 054423 (2009).
[28] Y. Kawaguchi, H. Saito and M. Ueda, Phys. Rev. Lett. **96**, 080405 (2006); Phys. Rev. Lett. **97**, 130404 (2006).
[29] S. Yi and H. Pu, Phys. Rev. Lett. **97**, 020401 (2006).
[30] L. Landau and E. Lifshitz, Phys. Z. Sowjetunion **8**, 153 (1935).

- [31] A. Hubert and R. Schäfer, *Magnetic Domains*, (Springer-Ferlag, Berlin 1998).
- [32] J. M. Deutsch and T. Mai, Phys Rev. E **72**, 016115 (2005).
- [33] F. Gerbier, A. Widera, S. Fölling, O. Mandel, I. Bloch, Phys. Rev. A **73**, 041602(R) (2006).
- [34] M. Tsubota, K. Kasamatsu, and M. Ueda, Phys. Rev. A **65**, 023603 (2002); K. Kasamatsu, M. Tsubota, and M. Ueda, Phys. Rev. A **67**, 033610 (2003).
- [35] S. Choi, S.A. Morgan, and K. Burnett, Phys. Rev. A **57**, 4057 (1998).
- [36] Y. Kawaguchi, H. Saito, K. Kudo, and M. Ueda, Phys. Rev. A **82**, 043627 (2010).
- [37] M. Ezawa, Phys. Rev. Lett. **105**, 197202 (2010).
- [38] Y.-J. Lin, R. L. Compton, K. Jiménez-García, J. V. Porto, and I. B. Spielman, Nature **462**, 628 (2009).